A Theory of Rotating Stall of Multistage Axial Compressors: Part III—Limit Cycles[1]

F. K. Moore
Sibley School of Mechanical and Aerospace Engineering, Cornell University, Ithaca, N.Y. 14853

A theory of rotating stall, based on single parameters for blade-passage lag and external-flow lag and a given compressor characteristic yields limit cycles in velocity space. These limit cycles are governed by Liénard's equation with the characteristic playing the role of nonlinear damping function. Cyclic integrals of the solution determine stall propagation speed and the effect of rotating stall on average performance. Solution with various line-segment characteristics and various throttle settings are found and discussed. There is generally a limiting flow coefficient beyond which no solution is possible; this probably represents stall recovery. This recovery point is independent of internal compressor lag, but does depend on external lags and on the height-to-width ratio of the diagram. Tall diagrams and small external lags (inlet and diffusor) favor recovery. Suggestions for future theoretical and experimental research are discussed.

Introduction

In Part I, it was shown [1] that a simple time lag of blade-passage force, accumlated in a multistage compressor and suitably matched with lags arising in entrance and exit flows, permits rotating stall as a kind of eigensolution of the equations for weak disturbances. A prediction of stall propagation and speed results, and it agrees well with the experiment discussed by Day, Greitzer and Cumpsty (D.G.C.) [3].

In Part II, finite amplitude disturbances were considered [2] in conjunction with compressor characteristics (upstream total to downstream static pressure rise, versus axial flow coefficient) which have parabolic shape over the range of fluctuation. It was found that, if the characteristic diagram is flat, the linear, harmonic solution of Part I applies, presumably limited by resistance to reverse flow. If the diagram is concave the disturbance wave is distorted, with the reduced-flow (stall) zone being steeper at its trailing edge, as observed by D.G.C. If the diagram is convex, as at stall inception, the disturbance is of limited amplitude, especially for multiple-zone stalls when the lag is negative. In this case, propagation speed would exceed 50 percent of wheel speed. These last results may relate to "progressive stall" often observed near the inception point.

None of the foregoing results indicate "recovery"; clearly, a more complete diagram must be used, incorporating unstalled and probably, reversed-flow segments. Use of a more complete diagram should also provide estimates of the effect of the presence of rotating stall on the average compressor performance. This, then, is the theme of this paper, to analyze the recovery phenomenon and other results which would come from using a complete performance diagram, and allowing oscillations to enter both unstalled and reverse-flow regions. We will find "limit cycles" which are more complex than the circles in phase space which arose in Parts I and II, and, under certain conditions, these limit cycles will appear to describe "relaxation oscillations," which we will argue represent recovery from rotating stall. Throughout, simple assumptions about internal and external lags will be maintained as in Parts I and II.

Notation is the same as that defined in Parts I and II; new quantities appear in the Nomenclature.

Support for this work by NASA-Lewis Research Center, during the author's sabbatic leave from Cornell is gratefully acknowledged, as well as helpful discussions with C. L. Ball and L. Reid of NASA, and E. M. Greitzer of MIT.

The Cycle Equation

We return to the basic equation (1) of Part II. It permits finite amplitude disturbances of axial velocity (g) and transverse velocity (h) at entrance, as functions of angle (θ) around the compressor. Assuming zero entrance loss at the IGV entrance

$$\lambda g'(\theta) - mfh + \Psi - \psi_c(\phi) = 0 \qquad (1)$$

Lags are embodied in the parameters, λ and mf, where f is propagation speed coefficient, and m reflects inlet and outlet flow lags; if the exit flow is a sudden expansion, and entrance flow is potential, then $m = 1$. If the exit is a straight duct, then we know only that $m = 2$ for small disturbances. We assume that m is constant for large disturbances as well, with $m = 2$ being appropriate for compressors followed by long diffusers. Research is needed to give a more complete picture of exit lag effects. Here, we will show the importance of m, or the

[1] Research done at Lewis Research Center, Cleveland, Ohio.

Contributed by the Gas Turbine Division of THE AMERICAN SOCIETY OF MECHANICAL ENGINEERS and presented at the 28th International Gas Turbine Conference and Exhibit, Phoenix, Arizona, March 27-31, 1983. Manuscript received at ASME Headquarters December 20, 1983. Paper No. 83-GT-46.

phenomena it imperfectly represents, for rotating stall. The compressor lag is embodied in the parameter λ, also related to f according to equation (16) to follow.

The last two terms of equation (1) refer to the compressor diagram, sketched in Fig. 1. To define $\psi_c(\phi)$, we imagine a test in which ϕ is varied from design to reverse flow, but rotating stall is suppressed by forcing axial velocity to remain circumferentially uniform (a high-drag screen at exit would work, in principle). In that case, ψ_c would be the characteristic measured in the absence of rotating stall. An operating point of the compressor (with axial velocity no longer constrained to be constant) would lie on a throttle line, but at Ψ, either above or below the characteristic. Thus, δ represents the effect of rotating stall on performance at a given average flow coefficient $\phi=\Phi$. It will be convenient to define the characteristic function relative to the intersection of $\psi_c(\phi)$ and $\phi=\Phi$. Thus

$$\Psi-\psi_c(0)\equiv\delta;\psi_c(\phi)-\psi_c(0)\equiv G(g) \tag{2}$$

and equation (1) becomes

$$\lambda g'(\theta)-mfh-G+\delta=0 \tag{3}$$

This is the equation to be solved in this paper.

If one finds the disturbance functions $g(\theta)$ and $h(\theta)$, the disturbance of static-pressure rise through the compressor can be found from equation (18) of Part II. Aside from constants, relative to ρU^2 it is

$$C_p=-mfh+\Phi g+\frac{1}{2}(g^2+h^2) \tag{4}$$

This formula assumes full pressure recovery at the IGV entrance.

Relation of h to g. In order to solve equation (3) it is necessary to connect the functions h and g. If the upstream flow is potential flow in a straight duct, then $h(\theta)$ is the Hilbert transform of $g(\theta)$, given for periodic functions by equation (17) of Part I

$$h=-\frac{1}{\pi}\int_0^{2\pi} g'(\xi)\ln\left|\sin\frac{\theta-\xi}{2}\right|d\xi \tag{5}$$

Because g is defined as a difference from average axial velocity, the average $\oint g d\theta = 0$. It can be shown from equation (5) that it is also true that the average $\oint h d\theta = 0$. Physically, this means that no swirl can be created in the entering potential flow.

Although equation (5) could be numerically incorporated into equation (3), it would be desirable to use some simpler relation, such as the one which is valid for single-cell stall and small perturbations, according to equation (19) of Part I, with $n=1$

$$h'(\theta)=-g \tag{6}$$

This equation is true for the first terms of Fourier series derivable from equation (5); in other words, it is exact if g is purely harmonic. Because we are concerned with "deep stall" in this paper, for which experiments [3, 6] show single-cell stall, we will assume $n=1$. Actually, results for higher modes can be inferred by substituting the appropriate multiple of wheel diameter in the parameter, a, of equation (16) to follow.

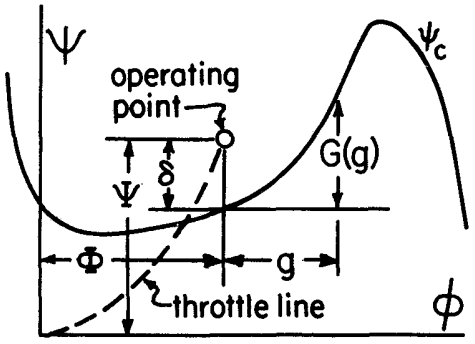

Fig. 1 Sketch of notation on compressor performance diagram, of total-to-static pressure rise (ψ_c) versus flow coefficient (ϕ) in absence of rotating stall. Operating point in rotating stall is δ above steady diagram.

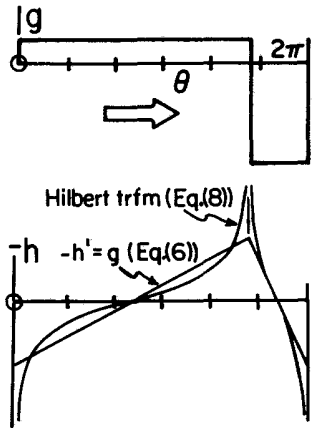

Fig. 2 Comparison of correct determination of h from g (equation (8)) with generally approximate equation (6) for a step wave (β = 0.8)

The nonlinear solution, equation (6*b*) of Part II, can be manipulated to yield

$$h'=-\left(1-2\frac{\eta}{A}h\right)g \tag{7}$$

and one could consider making more general use of such a nonlinear relation in equation (3), rather than equation (6).

We shall see that a "blockage" function has particular relevance to recovery. That is, $g(\theta)$ might be a step function as shown in Fig. 2. The example chosen has a "blockage" of $1-\beta$ = 20 percent. Such a "relaxation oscillation" will

Nomenclature

A = amplitude, equation (8)
$\mathfrak{B}$ = width of characteristic, Fig. 4(*a*)
$\mathfrak{C}$ = rise of deep-stall line, Fig. 4(*a*)
$\mathfrak{D}$ = slant of unstalled leg, Fig. 4(*a*)
$\mathfrak{E}$ = slant of reverse-flow leg, Fig. 4(*a*)
$\mathfrak{F}$ = height of drop into stall, Fig. 4(*a*)
$G(g)$ = characteristic function, rotating stall absent, Figs. 1 and 4(*a*)
g = axial velocity disturbance, equation (4), Part I
h = circumferential velocity disturbance, equation (15) of Part I
β = throttle setting, Fig. 4(*a*)
δ = increment of performance due to rotating stall (Fig. 1)

Superscripts

$\hat{}$ = (caret) transformation defined by equation (11)
$\hat{\hat{}}$ = (double caret) after change of scale so that width of characteristic is 1

Subscript

cr = critical or recovery value

provide a severe test of the reasonableness of equation (6). Substitution into equation (5) gives the corresponding $h(\theta)$

$$h = \frac{A}{\pi\beta(1-\beta)} \ln \left| \frac{\sin\left(\frac{\theta}{2} - \pi\beta\right)}{\sin\frac{\theta}{2}} \right| \tag{8}$$

with A being the amplitude of the g oscillation. Equation (8) is shown on Fig. 2; the result is singular at the two values of θ where g jumps. For comparison, we show equation (6). Apparently, equation (6) represents the correct Hilbert transform quite well on the average. Equation (7) would be inappropriate because it would not have the correct antisymmetry about the midpoints of the stalled and unstalled zones. We are therefore emboldened to adopt equation (6) for general use in equation (3); it is correct in the small perturbation (harmonic) limit, and has the correct antisymmetry as well as a reasonable amplitude in the "blockage" limit.

Liénard's Equation. Equation (6) permits the transformation of equation (3) into a generalization of the classical van der Pol equation [4], with the characteristic function, $G(g)$, playing the role of damping function. From equation (6),

$$g'(\theta) = -g\, dg/dh \tag{9}$$

In phase space, equation (3) becomes

$$\lambda g g'(h) + mfh + G - \delta = 0 \tag{10}$$

The following transformations and shift of origin (and sign) of h

$$\left.\begin{aligned} \hat{G} &= \frac{G(g)}{(mf)^2};\quad \hat{\delta} \equiv \frac{\delta}{(mf)^2} \\ \hat{h} &\equiv -\frac{h}{mf} + \hat{\delta};\quad \hat{g} \equiv \frac{1}{mf}\sqrt{\frac{\lambda}{mf}}\, g \end{aligned}\right\} \tag{11}$$

yield a new expression for angle θ

$$d\theta = -\frac{dh}{g} = \sqrt{\frac{\lambda}{mf}}\,\frac{d\hat{h}}{\hat{g}} \tag{12}$$

and yield the Liénard equation [4]

$$\hat{g}\hat{g}'(\hat{h}) + \hat{h} = \hat{G}(\hat{g}) \tag{13}$$

Equation (12) provides, for a complete cycle

$$\oint \frac{d\hat{h}}{\hat{g}} = 2\pi\sqrt{\frac{mf}{\lambda}} \tag{14}$$

and the requirement $\oint h\, d\theta = 0$, where equations (11) and (12) are used, becomes

$$\oint \frac{\hat{h}\, d\hat{h}}{g} = \left(2\pi\sqrt{\frac{mf}{\lambda}}\right)\hat{\delta} \tag{15}$$

If $\hat{G}$ were given, equation (13) could be solved, and mf/λ found from equation (14). However, λ and f are related (equation (7) of Part II, neglecting effect of guide vanes for present purposes) by the definition

$$\lambda \equiv \frac{1}{a}\left(\frac{1}{2} - f\right);\quad a \equiv D/(2UN\tau) \tag{16}$$

where a is a reciprocal compressor time lag, in effect (equation (16), Part II). Therefore, f itself can be found. Then, the characteristic displacement $\hat{\delta}$ (or δ) comes from equation (15). Actually, of course, $G(g)$ would normally be given, rather than $\hat{G}(\hat{g})$, and therefore equations (13) and (14) would have to be solved simultaneously.

Under the foregoing transformations, equation (4) becomes

$$C_p = (mf)^2(\hat{h} - \hat{\delta}) + \Phi mf\sqrt{\frac{mf}{\lambda}}\,\hat{g} + \frac{(mf)^3}{2\lambda}\left[\hat{g}^2 + \frac{\lambda}{mf}(\hat{h} - \hat{\delta})^2\right] \tag{17}$$

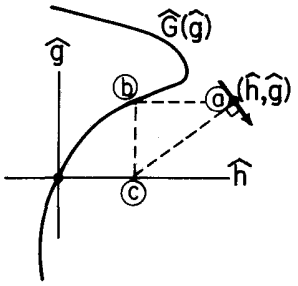

Fig. 3 Geometrical solution of the Liénard Equation (equation (13))

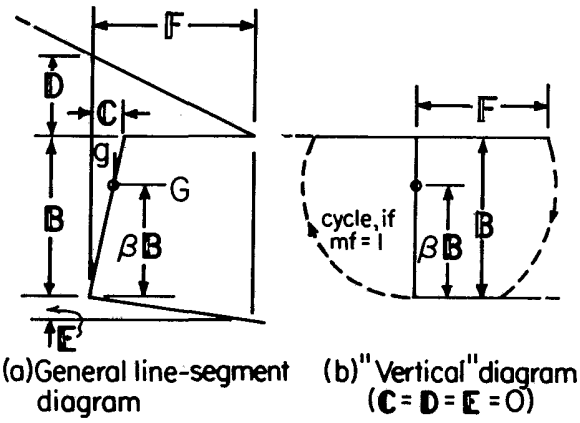

Fig. 4 Line-segment characteristic diagrams of function $G(g)$, oriented as in Fig. 3

Figure 3 sketches the usual geometrical construction for solving Liénard's equation [4]. The characteristic is reoriented (compare Fig. 1) to correspond to the classical damping function. Hereafter, in discussing solutions of equation (13), we will use this convention without further comment. At a point (a) during an oscillation, where the values $\hat{h}$ and $\hat{g}$ apply, one locates point (b), so that the line (a) – (b) has a length $\hat{h} - \hat{G}(\hat{g})$. The line (b) – (c) has the length $\hat{g}$. The negative reciprocal of the ratio of these lengths is, by equation (13) just $\hat{g}'(\hat{h})$ or the slope of the trajectory of the oscillation. Thus, that trajectory is locally perpendicular to the line (a) – (c), as sketched in Fig. 3. This geometrical method gives a quick sense of the progress of any oscillation in phase space.

Line-Segment Characteristic. In the rest of this paper, we will consider the function, G, to be various special cases of the line-segment diagram shown in Fig. 4(*a*). The quantities $\mathfrak{B}$ – $\mathfrak{F}$ are parameters of the diagram to be specified. The throttle setting is specified by β. We would usually consider the origin of ϕ to be at $\beta = 0$, so $\beta\,\mathfrak{B} = \Phi$.

A particularly simple but nontrivial case is sketched in Fig. 4(*b*). It is a "vertical" diagram in which the unstalled leg is vertical ($\mathfrak{D} = 0$) as is the reverse-flow leg ($\mathfrak{E} = 0$). The deep-stall leg is horizontal ($\mathfrak{C} = 0$). The circular arcs shown dashed in the sketch will be discussed later.

Some Limit-Cycle Examples

For purposes of illustration, we first pose a series of "indirect" problems, in which we specify $\hat{G}(\hat{g})$, find the resulting oscillation, determine f, and then infer the function $G(g)$. We note that equations (13–15) are invariant to a uniform change of scale. Thus, for example, we may imagine our diagram of $\hat{G}$ to be scaled so that its width is exactly 1; in

other words, so that $\hat{g} = g/\mathfrak{G}$. On this basis, we assume our diagrams of $\hat{G}$ to have width 1, with the scale of $\hat{h}$ suitably adjusted. Figure 5 shows a particular choice of diagram shape, double carets signifying the scale adjustment just discussed.

1 Suppose $\beta = 0.5$, and an oscillation begins at a point such as P. An analytic solution of equation (13) can easily be found for any part of an oscillation for which $\hat{G}(g)$ is a straight line, and these solutions can be pieced together to form a continuous trajectory in phase space. In this case, the trajectory is at first a growing spiral (the construction of Fig. 3 suggests this result directly) which grows until it encounters reverse-flow resistance, and then becomes momentarily "unstalled." After about three circuits, the oscillation becomes self-duplicating; that is, a "limit cycle" of the sort familiar in nonlinear mechanics, and in fact which is classically illustrated by van der Pol's equation with an S-shaped damping function. The usual compressor diagram, when properly oriented, is of that classical shape.

The initial amplification in this example is due to the deep-stall slope being positive. If it were negative, the oscillation would locally damp. In any case, the peak of $\hat{G}$ being to the right of the reverse-flow corner is amplifying, for an oscillation which is already strong enough. The slopes of unstalled and reverse-flow legs being negative are (locally) limiting. Thus, the oscillation, as it grows, ultimately settles into a limit cycle.

2 The limit cycle depends on the throttle setting (β) for a given diagram. Figure 6 shows the effect. Various symbols on the cycle traces serve to relate each trace to the value of β indicated in the legend and along the deep-stall line where each cycle is centered. It is noteworthy that if β is somewhat less than 0.5, the cycle is "caught" by reverse-flow resistance, but it never unstalls. As β is increased toward 1, the cycle is proportionately more unstalled, perhaps failing to be "caught" by the reverse-flow leg. As β approaches 1, the "release point" moves closer to the maximum-$\hat{G}$ corner, and, in fact, the unstalled part of the cycle tends to hug the unstalled leg of the diagram. If β is slightly greater than 1, the unstalled leg actually catches the trajectory before it reaches the corner, and a rapidly damped oscillation follows (because the unstalled leg has negative slope).

Table 1 shows the results when equations (14) and (15) are used to find f and hence $G(g)$ and δ. We assume $m = 2$, and $a = 1$, in order to make the example definite. The actual $\mathfrak{F}$ is only about 43 percent of $\mathfrak{G}$; rather a lightly loaded compressor. The value of f is about 0.26, tending to increase as β increases. As is obvious from Fig. 6, the δ needed to bring the average h to zero is greatest when $\beta = 0.5$; that cycle lies more to the right than the others.

Figure 7 shows the profiles of $g(\theta)$ which may be derived from Fig. 6 and equation (12). The wave is propagating to the right. Thus, the fraction of circumference with reduced flow becomes less as β increases, as one would expect. There is a tendency, not very strong, for the "trailing edge" of the reduced-flow (stall) zone to be steeper than the leading edge, for the lower flow rates, as observed by D.G.C. [1].

3 The limit cycle depends on the diagram "tallness." Figure 8 shows how the limit cycle changes when β is kept at 0.9, but the scale of $\hat{G}$ is changed by factors of 2 and 3 beyond the case shown in Fig. 6 (and repeated in Fig. 8 for comparison). Obviously, as scale of $\hat{G}$ increases, the cycle follows the unstalled leg very closely indeed, releasing just at the top point of the diagram in the limit. The reverse-flow leg is also

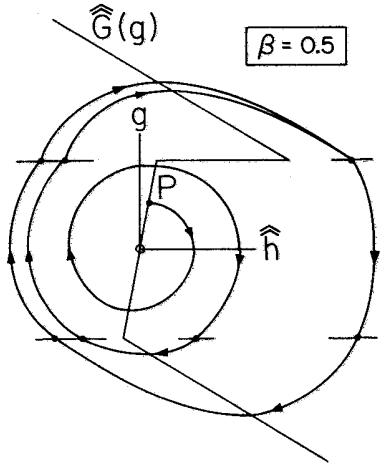

Fig. 5 Development of limit cycle for $\beta = 0.5$. Oscillation begins at point P. After three cycles, negligible changes. See Table 1 for diagram parameters corresponding to assumed $\hat{\hat{G}}(g)$.

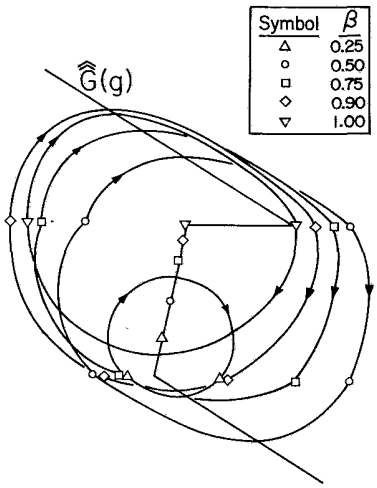

Fig. 6 Effect of throttle setting (β) on limit cycles; for the same given $\hat{\hat{G}}(g)$. See Table 1 for the corresponding diagram parameters.

Table 1 Results for limit-cycle examples[a]

Symbol	β	$\sqrt{\frac{mf}{\lambda}}$	$\hat{\hat{\delta}}$	f	$\sqrt{\lambda mf}$	$\mathfrak{F}/\mathfrak{G}$	$\delta/\mathfrak{F}$
△	0.25	1.028	0.043	0.26	0.50	0.45	0.048
○	0.50	1.076	0.221	0.26	0.60	0.45	0.246
□	0.75	1.084	0.190	0.26	0.50	0.45	0.121
◇	0.90	1.151	−0.032	0.29	0.50	0.45	−0.036
▽	1.00	1.336	0.068	0.32	0.48	0.43	0.076
◇	0.90	1.151	−0.032	0.28	0.50	0.45	−0.036
◇	0.90	1.178	0.387	0.37	0.44	0.78	0.215
◇	0.90	2.400	0.766	0.426	0.36	0.96	0.284

[a]Shapes of $\hat{\hat{G}}(g)$, as in Figs. 5 and 8, defined by reference to Fig. 4: $\hat{\mathfrak{G}} = 1$; $\hat{\mathfrak{D}} = \hat{\mathfrak{E}} = 9/16$; $\hat{\mathfrak{F}} = 0.9$; $\hat{\mathfrak{C}} = 0.2$. In Fig. 8, $\hat{\mathfrak{F}}$ and $\hat{\mathfrak{C}}$ multiplied by 1, 2, 3. $m = 2$, $a = 1$.

followed closely, and, again, release occurs close to the lower corner of the diagram. These effects of diagram tallness will be of great significance in our subsequent discussion of recovery.

The last three rows of Table 1 show the completed calculations. Even in the most extreme case, $\mathcal{F}$ is only about equal to $\mathcal{B}$. In that case, f has increased to 0.43, and δ has increased dramatically, as Fig. 8 suggests it should.

Figure 9 shows $g(\theta)$ for the most extreme case, to be compared with the profile $\beta = 0.9$ in Fig. 7. The stalled angle is reduced, and the expected steepness of the stall trailing edge is very definite. The intercepts of a horizontal line ($\hat{G} = 0$) with the unstalled and reversed legs are shown ("unstall g" and "reverse g" to indicate how well this profile conforms to blockage ideas, namely that the flow is either stalled or unstalled. The concept seems not to be very useful in this case. Also shown is the pressure-rise disturbance, C_p, obtained from equation (17), with $\mathcal{B}$ taken to be 1.

We proceed now to analysis of the direct problem, in which a simple "vertical" shape of $G(g)$ is given, and we will pay particular attention to indications of stall recovery as the throttle is opened.

Ideal-Diagram Solutions

Vertical Diagram. The "vertical" diagram of Fig. 4(b) has only $\mathcal{F}$ and $\mathcal{B}$ as parameters, and, because the equations are invariant to overall scale change, only the single parameter $\mathcal{F}/\mathcal{B}$ is significant, along with throttle setting β.

The limit cycle in this case is simply described in the h, $\hat{g}$ plane. Reference may be made to Fig. 4(b), imagining it to be transformed to $\hat{h}$ and $\hat{g}$, or as if $mf = 1$. Equation (13) tells us that the cycle follows the unstalled leg ($\hat{g}' = 0$) until the peak of $\mathcal{F}$ is reached ($\hat{h} = \hat{G}_{\max}$). The cycle leaves that corner, and is governed by $\hat{G}(\hat{g}) = 0$. In that part of the cycle, equation (13) is satisfied by a circular arc centered at (0, 0). It is shown dashed on Fig. 4(b). The arc will intersect the reverse-flow leg as shown, provided the diagram is tall enough.

In the $\hat{h}$, $\hat{g}$ plane, "tallness" will depend on f as well as $\mathcal{F}/\mathcal{B}$, because of the transformations, equations (11) and (12). The height-to-width ratio will be

$$\frac{\mathcal{F}/\mathcal{B}}{\sqrt{\lambda mf}}$$

in the $\hat{h}$, $\hat{g}$ plane. Thus, if f is near 0.5, so that λ is small, then any diagram will be "tall" in the $\hat{h}$, $\hat{g}$ plane, and, incidentally, the cycle will always reach the reverse-flow line.

The cycle will then follow the reverse flow line until the corner is reached at $\hat{h} = 0$. Then another circular arc governs the return to the unstalled condition. This second arc will reach the unstalled line only if $\beta > 0.5$. If $\beta < 0.5$, the arc will simply complete a circle back to the starting point. This solution corresponds to the purely harmonic wave (limited by reverse-flow resistance) discussed in Part II.

It is a simple matter to evaluate the cyclic integrals, equations (14) and (15) in these cases. Along the arc segments, the differential $d\hat{h}/\hat{g}$ is simply the angle increment along the arc. Therefore, according to equation (12), the real angle change, $d\theta$, is simply $\sqrt{\lambda/mf}$ times the angle of arc in the $\hat{h}$, $\hat{g}$ plane. An immediate conclusion may be drawn: Fig. 4(b) shows that the arc from unstalled to reverse condition generally subtends a smaller angle than the return. Therefore, the drop into stall is more abrupt than the recovery. Since the stall zone is traveling in the positive θ direction (Fig. 4 of Part I), the drop into stall is the "trailing edge" of the stall zone, in D.G.C.'s terminology [3], and, in keeping with their observations, the trailing edge of the zone is predicted always to be steeper than the "leading edge."

The foregoing simple calculations were made for various $\mathcal{F}/\mathcal{B}$, λ, and mf, subject to the requirement of equation (14), and finding δ from equation (15). Typical results are shown

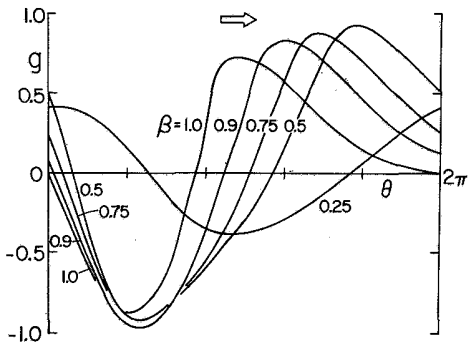

Fig. 7 Axial-velocity disturbance around the compressor for the various throttle settings given in Fig. 6. Here, $\mathcal{B} = 1$.

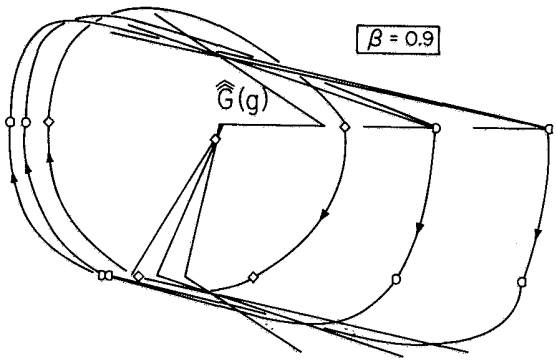

Fig. 8 Effect of changes of diagram height (scale of $\hat{G}$). See Table 1 for the numerical values.

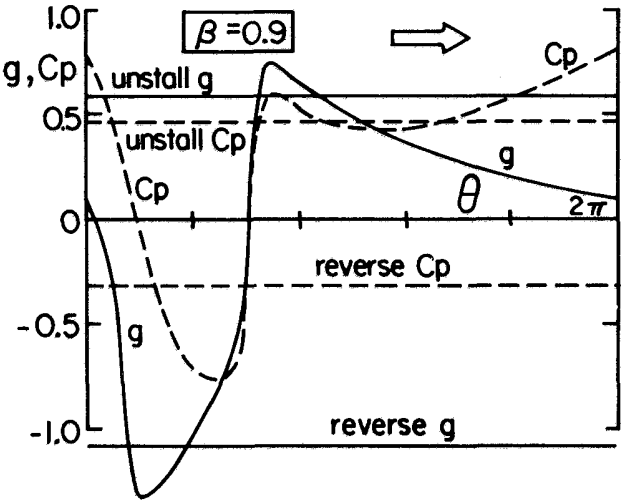

Fig. 9 Axial velocity (g), static pressure-rise (C_p) disturbances, for β = 0.9 and the most extreme case of Fig. 8 (Symbol ◇, see Table 1)

for $\mathcal{F}/\mathcal{B} = 1$ on Fig. 10. The solid-line results do not depend on compressor lag (a); only when the definition of λ (equation (16)) is introduced, overlaid on Fig. 10 as dot-dashed lines, does a become a factor. The intersections of dashed and solid lines provide the solution shown in Fig. 11 for the special cases of $m = 2$ and $a = 0.3$ and 0.6.

These solutions describe two regimes: The harmonic wave, for which $\delta = 0$, when $\beta < 0.5$, and a rather different wave when $\beta > 0.5$. The velocity, pressure-rise and phase diagrams for these two cases (with $a = 0.6$) are shown as the first and second rows of Fig. 12. The steeper "trailing edge" is evident in $g(\theta)$ for $\beta > 0.5$.

It is obvious from Fig. 10 that the external lag parameter

(m) is more significant than the internal one, especially for the larger values of β. The speed, f, is restricted to less than 0.5. Therefore, if m is small, say 1, rotating-stall solutions might be forbidden entirely. Even if $m=2$, no solution is possible when $\beta > 0.801$. In the next paragraphs, this point will be discussed more fully.

The Recovery Limit. When $m=2$, a limit is reached when $\beta=0.801$. At that limit, which is independent of a, the speed, f, goes to 0.5, and so does $\delta/\mathfrak{F}$. The third row of Fig. 12 shows the corresponding traces. The axial velocity becomes a pure step wave and the circumferential velocity is a saw tooth. (This type of "relaxation oscillation" was discussed earlier in connection with Fig. 2.)

The phase diagram becomes a rectangle because λ has approached zero. From equation (10) one would expect dg/dh to become infinite when $\lambda\to 0$. Another way to see this result is to recall that the cycle includes arcs in the $\hat{h}$, $\hat{g}$ plane, in which the diagram is infinitely "tall" when $\lambda\to 0$. That is, while g changes by $\mathfrak{G}$, equation (12) says that g changes only to order $\mathfrak{G}\sqrt{\lambda}$ when λ is small. Thus, the arcs depart to a vanishing degree from $\hat{h}=\mathfrak{F}/(1/2)\mathrm{m}$ when stalling or $\hat{h}=0$ when unstalling. The result in the original frame of reference is a rectangular cycle.

Pursuing further the effort to interpret the limiting solution physically, we may focus attention on equation (14). Essentially, it is the requirement that the cycle complete itself in the angular distance 2π. Now if we specify a large β, then $\hat{g}$ is a small constant quantity on the unstalled leg of the cycle. The coordinate $\hat{h}$ must change by a certain amount essentially fixed by the height of the diagram ($\mathfrak{F}$). Thus, the contribution of the unstalled leg to the integral $\oint d\hat{h}$ ($\hat{g}$ will be of the order $\mathfrak{F}/[(1-\beta)\mathfrak{G}\sqrt{\lambda}]$, and equation (14) suggests that if β is too near 1, the unstalled leg will use up all the allowed range of θ. Clearly, β may be permitted to be largest when the other terms of the integral are minimized. This occurs when the stalling and unstalling arcs have the least angle in the $\hat{h}$, $\hat{g}$ plane, namely zero when $\lambda\to 0$, and the negative-$\hat{h}$ portion of the unstalled leg is minimized; again, when $\lambda\to 0$. In the $\lambda\to 0$ limit, the reverse flow leg is longest, but $\hat{g}$ is larger there, and so the contribution to β is less important.

In summary, as the throttle is opened, a limiting condition is reached such that the cycle spends too much time unstalled to permit the required pressure changes of stalling and unstalling to occur. This description would seem to fit the phenomenon of "stall recovery" [3]. It is significant that δ is quite large (about $(1/2)\mathfrak{F}$) when the critical $\beta=\beta_{cr}$ is reached. If this is true, a discontinuity of Ψ is predicted to occur when $\beta=\beta_{cr}$. The geometry of Fig. 1 suggests that a slightly more open throttle line than that for β_{cr} would have no nearby performance line to intersect, and a jump across to the unstalled line (i.e., recovery from stall) would have to occur.

The value $\beta_{cr}=0.801$ applies only for a vertical characteristic with $\mathfrak{F}/\mathfrak{G}=1$ and $m=2$. The general results for a vertical characteristic are

$$\beta_{cr}(1-\beta_{cr})=\frac{\mathfrak{F}/\mathfrak{G}}{\pi m};\ \frac{\delta_{cr}}{\mathfrak{F}}=\frac{1}{2} \tag{18}$$

which appear as the lowest curves on Fig. 14. If the diagram is

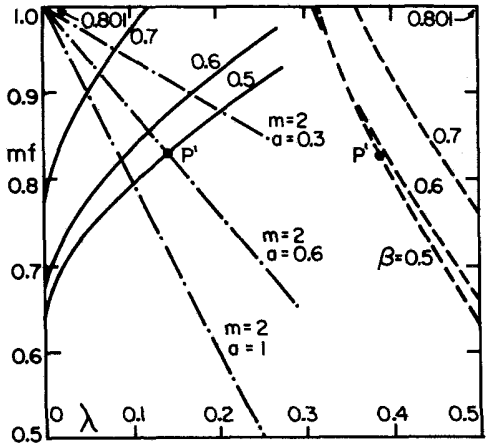

Fig. 10 λ and δ (shown dashed) versus mf for various β and $\mathfrak{F}/\mathfrak{G}=1$. The definition of $\lambda=(1/a)[(1/2)-f]$ overlaid (dot-dashed). Point P' gives the solution for $\beta=0.5$ when $a=0.6$, $m=2$.

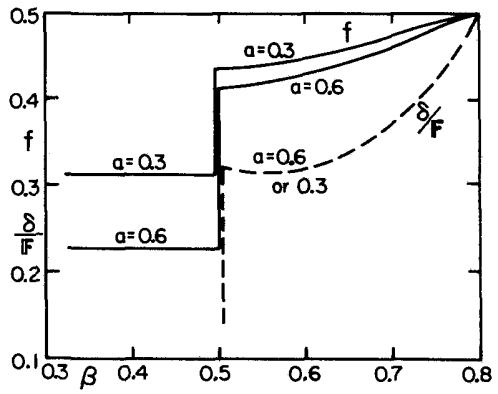

Fig. 11 Propagation speed (f) and performance rise due to rotating stall (δ) shown dashed versus throttle setting (β), for $m=2$ and $\mathfrak{F}/\mathfrak{G}=1$. No solution for $m=1$. Note that $\beta_{cr}=0.801$ is independent of lag (a), and that $\delta=0$ for $\beta<0.5$

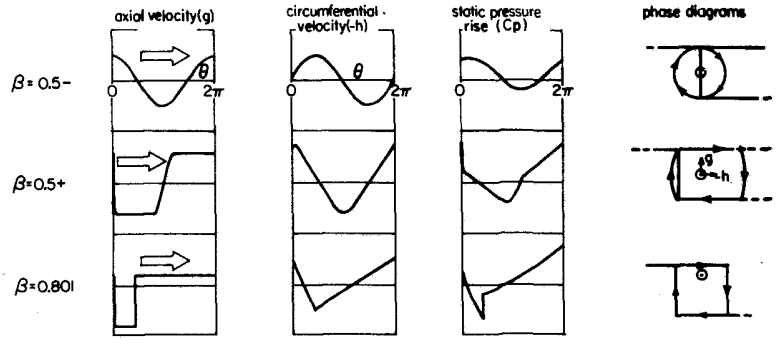

Fig. 12 Theoretical velocity and pressure "traces and phase diagrams for a particular vertical characteristic and three values of β ($\beta_{cr}=0.801$), $m=2$, $a=0.6$. Arrow denotes direction of propagation.

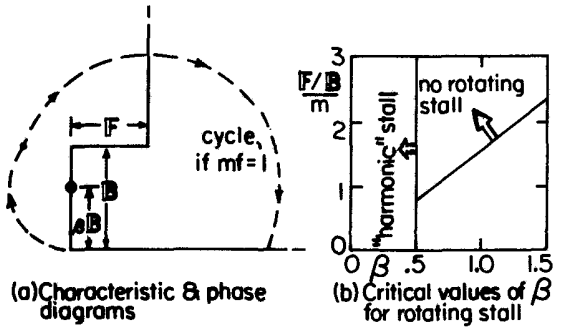

Fig. 13 Results for step-type characteristics, $m = 2$

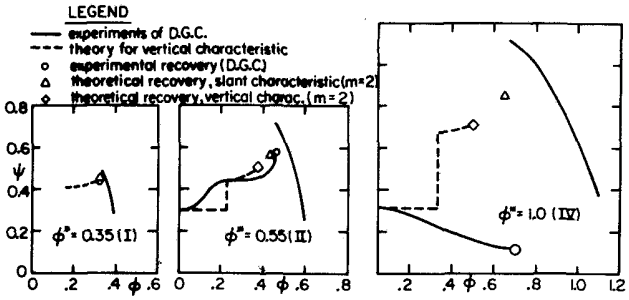

Fig. 15 Comparison of theoretical predictions with cases I, II, and IV (50 percent reaction) of Day, Greitzer and Cumpsty (D.G.C.), [3]

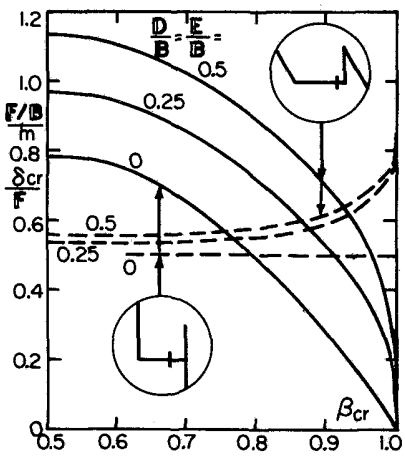

Fig. 14 Effect of slant characteristic on recovery throttle setting (β_{cr}) and performance rise at recovery (δ_{cr}), shown dashed, for $\mathcal{E} = \mathcal{D}$

less "tall," β_{cr} can approach 1. On the other hand, if $\mathcal{F}/\mathcal{G}$ exceeds $(1/4)\pi m$, no rotating stall other than the harmonic variety can occur.

In general, a tall diagram (large $\mathcal{F}/\mathcal{G}$) and a small value of m favor recovery. The role of m is particularly significant. We have inferred that m is about 2 for a compressor with a straight outlet. If m were reduced to 1 by using a sudden expansion, rotating stall could be largely suppressed, according to the present analysis, when $\mathcal{F}/\mathcal{G}$ is greater than about 0.8. Thus, changes in external lag mechanisms could be very effective for relatively "tall" diagrams, it would seem.

The Step Diagram. Another sort of ideal, simple diagram would continue to have $\mathcal{C} = \mathcal{E} = 0$, but $\mathcal{D} = \infty$ rather than 0. Figure 13(*a*) shows such a "step" diagram, together with a phase diagram in the $\hat{h}$, $\hat{g}$ plane (as if $mf = 1$). Such an extended unstalled plateau seems a possible model for Iura and Rannie's diagram [5], but is not typical of modern compressors.

The results show a lower, rather than an upper limit for rotating stall. It is

$$\beta_{cr} = 2\frac{\mathcal{F}/\mathcal{G}}{\pi m} \tag{19}$$

shown in Fig. 13(*b*). If the diagram is tall enough, there is a forbidden gap between $\beta = 0.5$ and β_{cr} where a rotating-stall solution is impossible. This is true only if $\mathcal{F}/\mathcal{G}$ exceeds $(1/4)\pi m$, which is quite tall. For smaller values of $\mathcal{F}/\mathcal{G}$, there is no critical case, and solutions for f are quite far from 0.5. For example, if $F/B = 0.5$, $m = 2$, and $a = 0.6$, the speed, f, would remain in quite a narrow range: 0.35 at $\beta = 0.5$ and 0.25 at $\beta = 1.5$.

Recovery for Line-Segment Characteristic

We now return to the more general line-segment characteristic shown in Fig. 4(*a*), and look for the effect to nonzero $\mathcal{C}$, $\mathcal{D}$, and $\mathcal{E}$. The general solution is easy to find, but hard to discuss because there are so many parameters to consider; the previous section describing Figs. 6–9 will suffice for illustration. If we consider only recovery, simplifications are available; f approaches 0.5, λ approaches 0, and compressor lag (*a*) become irrelevant.

As $\lambda \to 0$, we have seen how the transformation equation (12) makes the diagram "taller" in the $\hat{h}$, $\hat{g}$ plane without limit, so that, as in the vertical diagram case, the unstalling and stalling legs are lines of constant $\hat{h}$. The deep-stall slope, $\mathcal{C}$, becomes irrelevant except in finding δ, provided $\mathcal{C}$ is positive. If $\mathcal{C}$ is negative, the cycle would presumably follow the deep-stall leg and release at the corner $g = (1-\beta)\mathcal{G}$. We do not consider this possibility any further in the present paper. With $\mathcal{C} > 0$, the only change from the vertical-diagram analysis is that the integral of $d\hat{h}/\hat{g}$ must be carried out along the slanted lines defined by $\mathcal{D}$ and $\mathcal{E}$. When this is done, the following formulas for recovery result

$$\frac{\mathcal{F}/\mathcal{G}}{\pi m} = 1/\ln\left[\left(1+\frac{\mathcal{D}/\mathcal{G}}{1-\beta_{cr}}\right)^{\mathcal{G}/\mathcal{D}}\left(1+\frac{\mathcal{E}/\mathcal{G}}{\beta_{cr}}\right)^{\mathcal{G}/\mathcal{E}}\right] \tag{20}$$

$$\frac{\delta_{cr}}{\mathcal{F}} = \frac{\mathcal{F}/\mathcal{G}}{\pi m}\left[\frac{1-\beta_{cr}+\mathcal{D}/\mathcal{G}}{(\mathcal{D}/\mathcal{G})^2}\ln\left(1+\frac{\mathcal{D}/\mathcal{G}}{1-\beta_{cr}}\right)-\frac{\mathcal{G}}{\mathcal{D}}\right.$$
$$\left.+\frac{\beta_{cr}+\mathcal{E}/\mathcal{G}}{(\mathcal{E}/\mathcal{G})^2}\ln\left(1+\frac{\mathcal{E}/\mathcal{G}}{\beta_{cr}}\right)-\frac{\mathcal{G}}{\mathcal{E}}\right] \tag{21}$$

These formulas reduce to equation (18) when $\mathcal{E}$ and $\mathcal{D}$ are set equal to zero. The formula for δ is valid even if $\mathcal{C}$ is not zero, so long as δ is measured from the reverse flow corner at $g = -\beta\mathcal{G}$.

Figure 14 shows the effect of "slant," choosing $\mathcal{D} = \mathcal{E}$ for convenience. Clearly, slant increases the value of β_{cr}; in other words, it delays recovery. It remains true, however, that a tall diagram with small m will favor recovery. Figure 14 shows how the maximum value of $\mathcal{F}/m\mathcal{G}$, which occurs at $\beta_{cr} = 0.5$, depends on the slant parameter $\mathcal{D}/\mathcal{G}$. The more slanted the characteristic, the taller may be the diagram before the rotating-stall limit descends to $\beta_{cr} = 0.5$. Figure 14 also suggests that for realistic slants of about 0.5, recovery occurs in a fairly narrow range of β (between 0.9 and 1.0 for $\mathcal{F}/\mathcal{G} < 0.7m$). In D.G.C. [3], it is suggested that experiments indicate reccovery when a certain critical blockage (about 0.7) occurs. The present analysis is not quite consistent with this idea because β_{cr} is not the same as blockage. If β_{cr} is near 1, and $\mathcal{D}/\mathcal{G} = 0.4$, then the two ideas do happen to agree.

The dashed lines of Fig. 14 show that δ_{cr} is not greatly affected by slant unless β_{cr} is quite near 1. Of course, that is the region where recovery is generally predicted.

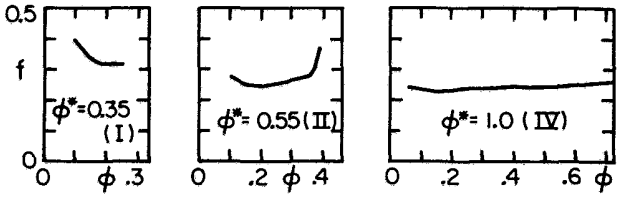

Fig. 16 Propagation speed versus flow coefficient for cases I, II, and IV shown on Fig. 15 (from Fig. 18 of Day's thesis [6]). Right margin of each diagram is at recovery value of ϕ.

Comparison With Experiment

Comparison of the present theory with experiment is handicapped by ignorance of the rotating-stall-free characteristic $\psi_c(\phi)$. In prinicple, it could be measured, but heretofore there has not been sufficient reason to do so. Nevertheless, in Part I, it was shown that theoretical predictions of propagation speed (f) agreed well with experiment. Here, we are concerned chiefly with recovery, and we may appeal to D.G.C. [3] for evidence.

Recovery. Figure 15 shows characteristics measured and reported by D.G.C. These appear as solid lines, with the recovery point indicated by a circle. Three different loadings are included, all at 50 percent reaction. For theoretical predictions, we have assumed that the shutoff head describes a constant value of deep-stall, ψ_c and calculated values of δ are applied relative to that level of ψ_c.

Therefore, if vertical diagrams were used, the theory would follow the dashed lines shown in each of the three cases. The average slant of the unstalled leg gives a basis for estimating the recovery point by use of equations (20) and (21). These points are triangles, and are presumably better estimates than the diamonds which terminate the vertical-characteristic results.

The "low-ϕ^*" (Case I) results are not very informative. The "intermediate-ϕ^*" (Case II) results show excellent agreement, even including a suggestion of transition from harmonic to limit-cycle waves. The "high-ϕ^*" (Case IV) is reasonable as regards β_{cr}, but quite poor as regards vertical shift of Ψ. Probably, the slope, $\mathcal{C}$, of the deep-stall ψ_c, should be taken as negative. If so, the integral, $\oint d\hat{h}/\hat{g}$, should be recalculated. It seems doubtful, however, that such a revision would give such a low value of Ψ at recovery. Perhaps the throttle plays a special role in recovery when the characteristic descends to such a low limit.

In all cases, it is worth noting that recovery, both in theory and experiment, is close to the break-point of the characteristic. That is, $\beta \approx 0.95$ at recovery. Perhaps this may prove a more basic concept than blockage.

Propagation Speed. Figure 16 shows the propagation speeds which correspond to the Cases I, II, and IV of Fig. 15. These speeds, given in Day's thesis [6], relate to theory just as recovery does in Fig. 15, if we recall that f should approach 0.5 ($\lambda \to 0$) at recovery, according to Fig. 11.

The low-ϕ^* Case I does not show the predicted rise of f toward 0.5, but the measurements do not extend to recovery; perhaps the rise would indeed occur if recovery were more closely approached.

The intermediate-ϕ^* Case II does show the predicted rise; perhaps the good agreement in this case is related to the good agreement of recovery prediction and experiment shown for Case II in Fig. 15. The high-ϕ^* Case IV shows the least agreement; the experiments show no rise, all the way up to recovery. Possibly this is an effect of throttle characteristic.

Iura and Rannie [5] also report a propagation speed which remains nearly constant right up to recovery. In their experiments, the compressor has an extended plateau of pressure beyond the stall point, somewhat like the steep characteristic of Fig. 13. In that case, we would in fact predict a nearly flat value of f.

Further comparisons of theory with experiment will require, on the one hand, a more thorough theoretical exploration of the parameters of the problem, and on the other hand, new measurements of rotating-stall-free compressor characteristic maps.

Concluding Remarks

The problem of rotating stall has been difficult largely because it occurs in such a complex parameter space. Perhaps the best service theory can provide in such a situation is to suggest priorities among these parameters, rather than to predict the resulting phenomenon in detail. The present set of three reports is set forth in this spirit. The most important results seem to be the following:

1 The recovery from rotating stall seems basically predictable. It depends on the compressor's steady characteristic; primarily its "tallness" (the height of the drop into stall compared with the diagram width), and secondarily the slope of the unstalled characteristic. Tallness favors early recovery. The slope of the reverse-flow resistance is of minor significance, as is the slope of the deep stall line, provided that slope is positive. If it is negative, the throttle curve may be important; otherwise, the throttle characteristic is unimportant.

Recovery does not depend on compressor lag (dynamic hysteresis), but it depends very much on the lags originating in the entrance and exit flows. Small external lags favor recovery. It seems likely that the most directly effective design change would be to reduce the lag in the exit duct.

2 The characteristic with rotating stall suppressed must be found experimentally to form a proper basis for further theoretical refinements. Discharge to a very low pressure through a dense screen at exit would force circumferentially uniform axial flow, and suppress rotating stall. Also, it would be important to suppress any effects of finite throttle-line slope, such as steady hysteresis about stall. Again, discharge to a low pressure would tend to steepen the throttle lines in the necessary way.

3 Research is needed on entrance flow fields and, especially, diffusers with transversely nonuniform flow. Dynamic (lag) effects are very important, more so than compressor blade-row dynamics.

4 Theoretical limit-cycle analysis can easily be extended to include a wider class of hypothetical characteristic diagrams, and a certain "exact" entrance and exit-flow relation. It is felt that these should proceed in parallel with the studies discussed in 2 and 3 above.

References

1 Moore, F. K., "A Theory of Rotating Stall of Multistage Axial Compressors, Part I. Small Disturbances," ASME Paper No. 83-GT-44, 28th International Gas Turbine Conference, Mar. 1983, pp. 313–320.

2 Ibid. Part II. "Finite Disturbances," ASME Paper No. 83-GT-45.

3 Day, I. J., Greitzer, E. M., and Cumpsty, N. A., "Prediction of Compressor Performance in Rotating Stall," ASME JOURNAL OF ENGINEERING FOR POWER, Vol. 100, Jan. 1978, p. 1–14.

4 Stoker, J. J., *Nonlinear Vibrations in Mechanical and Electrical Systems*, Interscience, New York (1970), ch. 5.

5 Iura, T., and Rannie, W. D., "Experimental Investigations of Propagating Stall in Axial-Flow Compressors," ASME *Transactions*, Apr. 1954, pp. 463–471.

6 Day, I. J., "Axial Compressor Stall," Ph.D. dissertation, Cambridge University Engineering Department, 1976.